



Evidence of Fenton-like reaction with active chlorine during the electrocatalytic oxidation of Acid Yellow 36 azo dye with Ir-Sn-Sb oxide anode in the presence of iron ion

Zaira G. Aguilar^a, Enric Brillas^b, Mercedes Salazar^c, José L. Nava^{a,*}, Ignasi Sirés^{b,*}

^a Departamento de Ingeniería Geomática e Hidráulica, Universidad de Guanajuato, Av. Juárez 77, Zona Centro, C.P. 36000 Guanajuato, Guanajuato, Mexico

^b Laboratori d'Electroquímica dels Materials i del Medi Ambient, Departament de Química Física, Facultat de Química, Universitat de Barcelona, Martí i Franquès 1-11, 08028 Barcelona, Spain

^c Departamento de Ingeniería en Minas, Metalurgia y Geología, Universidad de Guanajuato, ExHacienda San Matías S/N, C.P. 36020, Guanajuato, Guanajuato, Mexico

ARTICLE INFO

Article history:

Received 18 November 2016

Received in revised form 1 January 2017

Accepted 3 January 2017

Available online xxx

Keywords:

Azo dye

Mixed metal oxide

Electrochemical oxidation

Hydroxyl radical

Fenton-like process

Wastewater treatment

ABSTRACT

The degradation of 2.5 L of Acid Yellow 36 solutions at pH 3.0 by electro-oxidation (EO) has been studied in a flow plant with a reactor containing an Ir-Sn-Sb oxide anode and a stainless steel cathode. The anode was prepared onto Ti by the Pechini method and characterized by SEM-EDX and XRD. It showed a certain ability to electrocatalyze both, the generation of adsorbed $\bullet\text{OH}$ from water oxidation in sulfate medium and, more largely, the production of active chlorine in a mixed electrolyte containing Cl^- ion. The EO treatment of the dye solution in the latter medium led to a rapid decolorization because active chlorine destroyed the colored by-products formed, but color removal was much slower in pure NaClO_4 or Na_2SO_4 due to the limited formation of $\bullet\text{OH}$. In contrast, greater mineralization was obtained in both pure electrolytes since the by-products formed in the presence of Cl^- became largely persistent. The effect of liquid flow rate, current density and dye content on the EO performance in the mixed electrolyte was examined. The drop of absorbance and dye concentration obeyed a pseudo-first-order kinetics. Interestingly, the decolorization rate, dye concentration decay and TOC removal were enhanced upon catalysis with 1.0 mM Fe^{2+} . Such better performance can be accounted for by the formation of $\bullet\text{OH}$ in the bulk from the electro-Fenton-like reaction between electrogenerated HClO and added Fe^{2+} . Even larger mineralization was achieved by the photoelectro-Fenton-like process upon irradiation of the solution with UVA light due to photolysis of some refractory intermediates. Maleic and acetic acids were detected as final short-chain linear carboxylic acids. The loss of Cl^- and the formation of ClO_3^- , ClO_4^- , SO_4^{2-} , NO_3^- and NH_4^+ were evaluated as well.

© 2016 Published by Elsevier Ltd.

1. Introduction

About 70% of the world dye production corresponds to azo compounds [1], which have a complex chemical structure containing one or various azo groups ($-\text{N}=\text{N}-$) as chromophore, linked to aromatic systems with lateral groups including $-\text{OH}$, $-\text{CH}_3$ and $-\text{SO}_3^-$, among others [2–4]. These dyes are extensively employed in textile industries, which are highly polluting in terms of the color, volume and complexity of their discharged effluents [5,6]. Dye wastewater contains dye concentrations up to 250 mg L^{-1} , along with other toxic components, thus causing aesthetic problems, scarce light penetration and health problems to aquatic organisms owing to their carcinogenic, toxic and mutagenic properties [7,8]. The resistance to biodegradation and poor destruction of these pollutants by conventional treatments in wastewater treatment plants explain their large persistence in the aquatic environment [4,9,10]. Research is thus focusing on the development of more powerful treatments to remove

azo dyes from wastewater in order to avoid their hazardous effects on living beings.

Several electrochemical advanced oxidation processes (EAOPs), including electro-oxidation (EO, also called electrochemical oxidation or anodic oxidation) and processes based on Fenton's reaction like electro-Fenton (EF), have been recently utilized to efficiently destroy azo dyes [4,11–30]. EAOPs are easy to handle and very versatile, also presenting high energy efficiency, great effectiveness to oxidize organic pollutants and environmental compatibility. They show great ability for the in situ production of reactive oxygen species (ROS), like hydroxyl radical ($\bullet\text{OH}$) with such a high oxidation power ($E^\circ = 2.80 \text{ V/SHE}$) that it can non-selectively attack most organic pollutants until their mineralization [4,21,23,30].

EO is the simplest EAOP applied to wastewater treatment. The most basic setup consists in an electrolytic cell containing the polluted wastewater in contact with a cathode and a large O_2 -overvoltage anode (M) that catalyzes the generation of adsorbed $\text{M}(\bullet\text{OH})$ radical from water oxidation at high applied current density (j) as follows [31,32]:

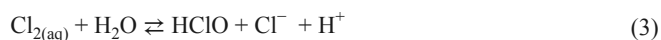


* Corresponding authors.

Email addresses: jlnm@ugto.mx (J.L. Nava); i.sires@ub.edu, isiresa@gmail.com (I. Sirés)

The production of $M(\bullet\text{OH})$ radical depends on the kind of anode. At so-called active anodes such as Pt, IrO_2 and RuO_2 , $M(\bullet\text{OH})$ is transformed into a less powerful oxidant like chemisorbed "superoxide" MO [19,33]. Such conversion can be minimized when using non-active anodes like PbO_2 , SnO_2 and boron-doped diamond (BDD), which promote high contents of physisorbed $M(\bullet\text{OH})$ leading to the mediated electrochemical incineration of organic pollutants on the anode [11,12,18,34,35]. It has been found that several active mixed metal oxide (MMO) anodes yield larger degradation than pure metal oxides, as reported for phenol and Reactive Orange 4 using $\text{Ti}/\text{SnO}_2\text{-Sb}_2\text{O}_3$ and $\text{Ti}/\text{SnO}_2\text{-Sb-Pt}$, respectively [36].

This general description is valid when the EO treatment is performed in the presence of anions like ClO_4^- , NO_3^- and SO_4^{2-} , which remain stable during the electrolysis or become a source of weak oxidants, e.g., $\text{S}_2\text{O}_8^{2-}$ at the BDD surface [31,32]. In contrast, the EO process becomes much more complex in the presence of Cl^- because it can be oxidized to active chlorine (Cl_2 , HClO and/or ClO^-) via Reactions (2)–(4), which competes with $M(\bullet\text{OH})$ to attack

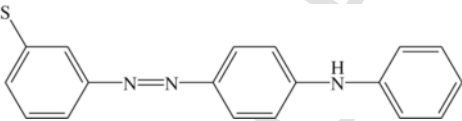


The predominant active chlorine species is $\text{Cl}_{2(\text{aq})}$ ($E^\circ = 1.36 \text{ V/SHE}$) until pH 3.0, HClO ($E^\circ = 1.49 \text{ V/SHE}$) within the pH range 3–8 and ClO^- ($E^\circ = 0.89 \text{ V vs. SHE}$) at pH > 8.0. The mediated electrochemical oxidation of organics with these species is then expected to be more successful in acidic medium. On the other hand, Kishimoto et al. [39] recently suggested the enhanced decontamination of acidic wastewater containing Cl^- through the generation of $\bullet\text{OH}$ in the bulk using Fe^{2+} and HClO via Fenton-like Reaction (5) [40]. Note that, actually, this corresponds to an EF-like process in which Reaction (5) replaces the classical Fenton's reaction between H_2O_2 and Fe^{2+} catalyst to form Fe^{3+} and $\bullet\text{OH}$ [4,23]. Reaction (5) can thus be sustained from Fe^{2+} regeneration upon cathodic reduction of Fe^{3+} via Reaction (6). Additionally, one could envisage the production of larger amounts of $\bullet\text{OH}$ from the photolytic reduction of $\text{Fe}(\text{OH})^{2+}$, the pre-eminent Fe^{3+} species at pH 3.0, by Reaction (7) upon use of UVA radiation [30,41]. The latter photoelectrocatalytic treatment, which is reported for the first time, can be so-called PEF-like process.



To give evidence of the upgrading of azo dye removal under EF-like and PEF-like conditions, we have undertaken a study on the degradation of Acid Yellow 36 in acidic chlorinated solutions using a purpose-made Ir-Sn-Sb oxide anode with ability to produce $M(\bullet\text{OH})$ radicals and active chlorine [38,42]. Acid Yellow 36 (also known as Metanil Yellow, see physicochemical properties in Table 1) has been chosen as model azo dye because it is present in wastewater from tex-

Table 1
Physicochemical properties of Acid Yellow 36 azo dye.

IUPAC name	Sodium 3-[(4-anilinophenyl)diazanyl]benzenesulfonate
Empirical formula	$\text{C}_{18}\text{H}_{14}\text{N}_3\text{NaO}_3\text{S}$
Molecular structure	
Color Index number	13,065
λ_{max}	437 nm
Molecular mass	$375.38 \text{ g mol}^{-1}$

tile, tannery, paper and cosmetic industries, among others. This refractory dye is a toxic and carcinogenic pollutant that causes mortality and adverse health effects in fishes [43]. Its consumption by humans causes toxic methaemoglobinaemia and cyanosis, whereas its contact with skin produces allergic dermatitis [44]. Effective decolorization and/or mineralization of synthetic Acid Yellow 36 solutions upon the action of $\bullet\text{OH}$ has been described by several AOPs including photocatalysis with TiO_2 [45,46] and ZnO [47], Fenton [48] and photo-Fenton [49]. EAOPs such as EO [50], EF [14,51] and PEF [15] with BDD anode, as well as PEF combined with TiO_2 photocatalysis [46], have also been employed but only in sulfate medium.

This article presents the results obtained for the degradation of a 0.46 mM Acid Yellow 36 solution (100 mg L^{-1} of total organic carbon (TOC)) in a 35 mM NaCl + 25 mM Na_2SO_4 mixture at pH 3.0 by EO. The experiments were performed in a 2.5 L flow plant with a filter-press cell equipped with an Ir-Sn-Sb oxide anode and a stainless steel cathode. The anode was composed of an MMO film onto Ti plate prepared by the Pechini method [52]. It was characterized by scanning electron microscopy with energy dispersive X-ray spectroscopy (SEM-EDX) and X-ray-diffraction (XRD), whereas its electrocatalytic ability to generate $\bullet\text{OH}$ and active chlorine was analyzed by electron paramagnetic resonance (EPR) and UV/vis spectroscopy, respectively. The effect of liquid flow rate, j and dye concentration on decolorization rate and mineralization degree was examined. Comparative trials using pure NaClO_4 or Na_2SO_4 as electrolyte were made to better assess the role of active chlorine in the mixed electrolyte. The influence of Fe^{2+} addition to the latter medium, either in the dark or under UVA irradiation, was studied to give strong evidence of the occurrence of a Fenton-like reaction. Intermediates and inorganic ions lost or released during the dye degradation were identified.

2. Materials and methods

2.1. Chemicals

Commercial Acid Yellow 36 (70% of dye content, the rest corresponding to inorganic products) was purchased from Sigma-Aldrich and used as received. The products for the MMO synthesis were $\text{H}_2\text{IrCl}_6 \cdot x\text{H}_2\text{O}$, SnCl_4 and SbCl_3 of analytical grade supplied by Sigma-Aldrich. The electrolytic solutions were prepared with deionized water and contained $\text{FeSO}_4 \cdot 7\text{H}_2\text{O}$, Na_2SO_4 , NaOH , NaCl and/or HClO_4 of analytical grade purchased from Fluka, Merck and Panreac. Analytical grade 5,5-dimethyl-1-pyrroline-*N*-oxide (DMPO) used for $\bullet\text{OH}$ detection was supplied by Sigma-Aldrich. Other chemicals were of either HPLC or analytical grade purchased from Fluka, Merck, Panreac and Sigma-Aldrich.

2.2. Synthesis of the mixed metal oxide electrode

Titanium plates were initially pretreated by dipping them into concentrated HCl at 70 °C for 1 h, followed by immersion in concentrated HNO₃ at room temperature for 15 min, rinsing with distilled water and drying at room temperature. This pretreatment increased the material roughness to improve the adhesion of oxides. The precursor polymer solution to apply the Pechini method was prepared by mixing citric acid and ethylene glycol with molar proportion of 0.00750:1 at 60–70 °C. After this, SbCl₃, SnCl₄ and H₂IrCl₆·xH₂O were added with molar proportion of 0.00012:0.00925:0.00925 for Sb:Sn:Ir, maintaining the temperature at 60–70 °C for 30 min, as optimized in one of our previous works [19]. The resulting solution was applied to the Ti substrate using a brush and the electrode was then heated at 115 °C for 15 min in a furnace for inducing the polymerization of the precursor, followed by heating at 550 °C for 10 min to calcinate the polymer and form the metal oxides. This procedure was repeated until achieving 32 coated layers, whereupon the electrode was heated at 550 °C for 1 h.

2.3. Bulk electrolysis

A scheme of the flow plant used in this work and constructed by us has been reported elsewhere [15]. The 2.5 L acidic dye solution was introduced in a reservoir and recirculated with a peristaltic pump, regulating the liquid flow rate with a flowmeter and the temperature at 30 °C with two heat exchangers. The electrochemical cell was a purpose-made filter-press-type reactor equipped with the prepared Ir-Sn-Sb oxide anode, a stainless steel plate cathode and a turbulence promoter Type D [35]. The anode and cathode area was 24 cm² (8 cm × 3 cm) and the interelectrode gap was 0.6 cm. The trials were carried out at constant *j* provided by a Grelco GVD310 power supply. An annular glass photoreactor containing an Omnilux 27E 160-W UVA lamp, connected between the reactor and reservoir, was used for the PEF-like assays. Most experiments were performed with a 0.46 mM Acid Yellow 36 solution in 35 mM NaCl + 25 mM Na₂SO₄. Several comparative assays were made with 50 mM NaClO₄ or 50 mM Na₂SO₄. The initial pH of the acidic solution was always adjusted to 3.0 because it has been found optimal for the treatments of organics by conventional EF [4,23].

2.4. Apparatus and analytical methods

The morphological characteristics and composition of the synthesized MMO film were assessed with 2.0 cm × 0.5 cm samples by SEM-EDX using a JSM-7100F field emission scanning electron microscope equipped with an INCA analyzer. The crystal structure was analyzed by XRD using a PANalytical X'Pert PRO MPD Alpha powder diffractometer in Bragg-Brentano $\theta/2\theta$ geometry with 240 mm radius. Reference diffraction patterns were selected from the ICDD database.

The hydroxyl radicals were detected by spin trapping, analyzing the *OH-DMPO adduct by EPR [53]. To do this, 10 mL of a 10 mM DMPO solution at pH 3.0 were electrolyzed in an undivided cell with a 1 cm² Ir-Sn-Sb oxide anode and a 1 cm² stainless steel cathode at *j* = 20 mA cm⁻² for 15 min under vigorous stirring with a magnetic bar at room temperature. The treated solution was immediately frozen with dry ice for preservation to be further analyzed by EPR with a Bruker ESP300E spectrometer, using Win-EPR and SimFonia 2.3 software.

Active chlorine was determined by the *N,N*-diethyl-*p*-phenylenediamine (DPD) colorimetric method using a Shimadzu 1800 UV/vis spectrophotometer set at $\lambda = 515$ nm [54]. The solution pH was determined with a Crison 2000 pH-meter. Color removal was monitored from the absorbance (*A*) decay of its main visible band at $\lambda_{\text{max}} = 437$ nm, related to the conjugated azo bond [15], using the above spectrophotometer. The percentage of color removal or decolorization efficiency was then calculated as follows [4]:

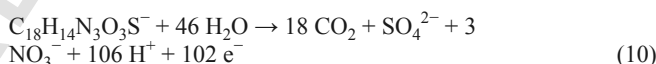
$$\text{Percentage of color removal} = \frac{A_0 - A}{A_0} \times 100 \quad (8)$$

where *A*₀ and *A* denote the absorbance of the initial solution and at time *t*, respectively.

Acid Yellow 36 mineralization was followed from the removal of solution TOC using a Shimadzu VCSN TOC analyzer. Samples withdrawn from initial and treated solutions were filtered with 0.45 μm PTFE filters purchased from Whatman and 50 μL aliquots were directly injected into the above analyzer, obtaining 1% accuracy in all triplicate measurements. TOC data allowed estimating the mineralization current efficiency (MCE) from Eq. (9) [15]:

$$\% \text{MCE} = \frac{n F V_s \Delta(\text{TOC})_{\text{exp}}}{4.32 \times 10^7 m I t} \times 100 \quad (9)$$

where *F* is the Faraday constant (96,485C mol⁻¹), *V*_s is the solution volume (L), $\Delta(\text{TOC})_{\text{exp}}$ represents the experimental TOC removal (mg L⁻¹), 4.32×10^7 is a conversion factor (3600 s h⁻¹ × 12000 mg C mol⁻¹), *m* = 18 is the number of carbon atoms of Acid Yellow 36, *I* is the applied current (A) and *t* is the electrolysis time (h). Considering the dye mineralization to CO₂ and SO₄²⁻ and NO₃⁻ ions, as will be discussed below, the number *n* of electrons required for the theoretical total mineralization of its anion form was taken as 102 from Eq. (10):



The dye decay kinetics was followed by reversed-phase high-performance liquid chromatography (HPLC) using a Waters 600 LC fitted with a BDS Hypersil C18 6 μm, 250 mm × 4.6 mm, column at 35 °C and coupled to a Waters 996 photodiode array detector selected at $\lambda = 437$ nm. The mobile phase was a 50:50 (v/v) acetonitrile/water (phosphate buffer of pH 3.0) mixture at 0.6 mL min⁻¹. Samples were diluted with the same volume of CH₃CN to stop the degradation of the dye. Aliquots of 20 μL were injected into the LC and the chromatograms exhibited a well-defined peak related to Acid Yellow 36 at retention time (*t*_r) of 5.6 min. Final carboxylic acids were quantified by ion-exclusion HPLC upon injection of 20 μL of the same samples to the above LC with a BioRad Aminex HPX 87H, 300 mm × 7.8 mm column, at 35 °C, selecting the photodiode array detector at $\lambda = 210$ nm. The mobile phase was 4 mM H₂SO₄ circulating at 0.6 mL min⁻¹. The recorded chromatograms displayed peaks associated with maleic acid at *t*_r = 8.1 min and acetic acid at *t*_r = 15.1 min.

The SO₄²⁻, Cl⁻, ClO₃⁻ and ClO₄⁻ concentrations in treated solutions were measured by ion chromatography upon injection of 25 μL aliquots into a Shimadzu 10Avp LC coupled to a Shimadzu CDD 10Avp conductivity detector. The LC was fitted with a Shim-Pack

IC-A1S, 100 mm × 4.6 mm, anionic column at 40 °C and the mobile phase was a 2.6 mM phthalic and 2.4 mM tris(hydroxymethyl)aminomethane (pH = 4.0) solution circulating at 1.5 mL min⁻¹. For NO₃⁻ determination, the mobile phase containing boric acid, sodium gluconate, sodium tetraborate, acetonitrile, butanol and glycerine was eluted at 2.0 mL min⁻¹. The NH₄⁺ content was measured spectrophotometrically according to the standard indophenol blue reaction.

3. Results and discussion

3.1. Characterization of the Ir-Sn-Sb oxide electrode

Fig. S1a of Supplementary material depicts representative SEM images at magnifications of 1000× and 20,000× for the Ir-Sn-Sb oxide coating onto the Ti substrate, as obtained by the Pechini method. A good coverage and high adherence was revealed to the naked eye. A compact and uniformly distributed oxide layer can be observed at 1000×, evidencing a certain roughness at 20,000×. The surface morphology presented some small cracks, as expected from thermal treatments that cause a rapid evolution of CO₂ gas formed by the decomposition of the organic polymer [19,55,56].

The metal content in the precursor solution (in atomic percent) was distributed as follows: 49.7 at.% Ir, 49.7 at.% Sn and 0.6 at.% Sb. Worth mentioning, the Ir/Sn/Sb molar ratio was preserved in the prepared film, since EDX analysis revealed that the final coating contained 11.3 at.% C, 64.1 at.% O, 2.6 at.% Cl, 10.0 at.% Ir, 12.0 at.% Sn and 0.06 at.% Sb in average. The presence of C and Cl is due to residues from the polymer precursor utilized.

Fig. S1b of Supplementary material depicts the XRD pattern, from 15° to 75°, of the electrode showing some crystallographic planes that can be related to Ti, Ir and a mixed Sn-Sb oxide. Ti metal peaks, which appear from the diffraction of the underlying substrate and not as a result of uncoated areas as confirmed from the absence of Ti peaks in the previous EDX analysis, are slightly shifted from the standard ones. This agrees with mechanical stress mainly induced by heating periods. On the other hand, a mixed metal oxide whose peaks differ from pure SnO₂ is clearly distinguished. According to the standard diffraction pattern database (ICDD: 04-011-7759), a mixed Sn-Sb oxide matches quite well. However, since neither IrO_x nor Sb₂O₅ have been found in the diffractograms, in contrast to other works reporting the preparation of Ir-Sn-Sb oxide coatings by thermal treatment, it seems more reasonable to assign these XRD peaks (1) to a highly intermixed Ir-Sn-Sb oxide that is present as a solid solution. This may be accounted for by the selected synthesis methodology, including annealing temperatures that favor the solid state diffusion of all metals to form the MMO. Note that at such high temperature, Ir is present not only as MMO, but some atoms segregate and appear as Ir metal as well. Although it is not easy to ensure the formation of Ir metal based on just a couple of peaks, this finding agrees with a work by Chen et al. [55].

3.2. Generation of hydroxyl radicals and active chlorine by the Ir-Sn-Sb oxide anode

Fig. 1a shows the EPR spectrum with the four characteristic bands of the •OH-DMPO adduct [53] that was detected when a 10 mM DMPO solution at pH 3.0 was electrolyzed with the synthesized Ir-Sn-Sb oxide anode at $j = 20 \text{ mA cm}^{-2}$ for 15 min. However, the bands were very weak, suggesting that the concentration of active M(•OH) generated at the anode surface was only slightly higher than $1 \times 10^{-8} \text{ M}$, the threshold value that can be measured by this technique. This means that, as in the case of pure IrO₂ mentioned in the

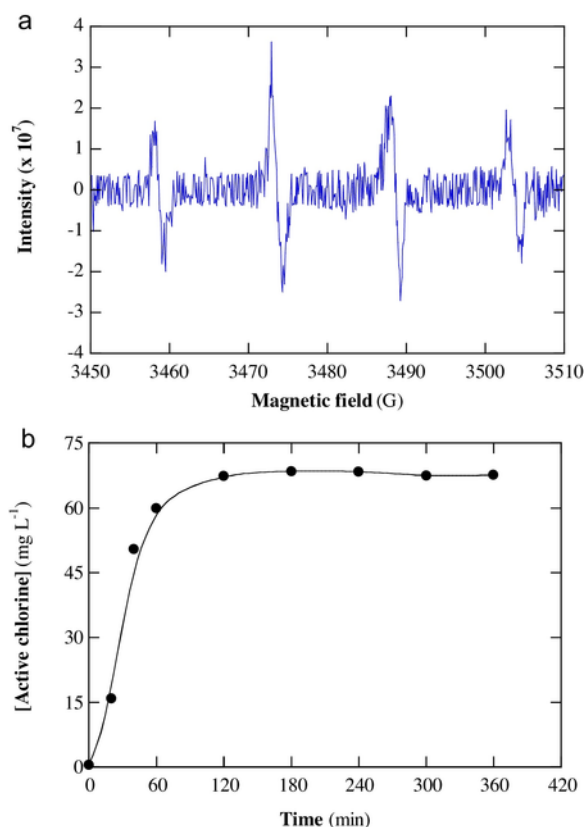
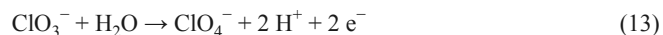
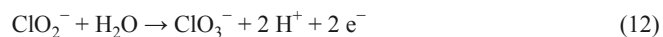
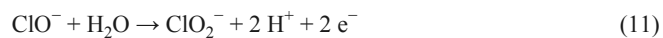


Fig. 1. (a) EPR spectrum of the •OH-DMPO adduct detected in 10 mL of a 10 mM DMPO solution in 0.05 M Na₂SO₄ at pH 3.0 and 30 °C. An Ir-Sn-Sb oxide anode and a stainless steel cathode were used, both of 1 cm², at a current density (j) of 20 mA cm⁻² for 15 min. (b) Active chlorine concentration vs. electrolysis time for the treatment of 2.5 L of a 35 mM NaCl + 25 mM Na₂SO₄ solution at pH 3.0 and 30 °C using the flow plant with an electrochemical reactor equipped with a 24 cm² Ir-Sn-Sb oxide anode and a 24 cm² stainless steel electrode at $j = 150 \text{ mA cm}^{-2}$ and liquid flow rate of 200 L h⁻¹.

introduction section, the Ir-Sn-Sb oxide could be considered an “active” anode in EO, possessing a low ability to oxidize organic pollutants by chemisorbed M(•OH).

In contrast, Fig. 1b depicts a large accumulation of active chlorine in 2.5 L of a 35 mM NaCl + 25 mM Na₂SO₄ solution at pH 3.0 upon treatment in the flow plant with the reactor equipped with the prepared Ir-Sn-Sb oxide anode and a stainless steel cathode at $j = 150 \text{ mA cm}^{-2}$. As can be seen, a quasi-steady active chlorine concentration near 68 mg L⁻¹ was obtained after 120 min of electrolysis. This is expected to occur exactly when the generation rate of this species from Cl⁻ oxidation by Reactions (2) and (3) becomes equal to its destruction rate, which is mainly due to its •OH-mediated or direct oxidation to ClO₂⁻, ClO₃⁻ and ClO₄⁻ ions via Reactions (11)–(13), as well as its cathodic reduction to Cl⁻ via Reaction (14) [4,24]:



Based on the above results, active chlorine (HClO at pH 3.0) is expected to be the pre-eminent oxidizing agent of Acid Yellow 36 and its by-products when treating 2.5 L of a dye solution by EO in the flow plant using the synthesized MMO anode in the presence of Cl^- at acidic pH, as presented in subsections below.

3.3. Influence of the electrolyte on the electro-oxidation of acid yellow 36 solutions

A first series of experiments was made to ascertain the decolorization and mineralization power of $\text{M}(\bullet\text{OH})$ and active chlorine for the removal of Acid Yellow 36 and its by-products. Independent solutions of 0.46 mM of dye in either 50 mM NaClO_4 , 50 mM Na_2SO_4 or 35 mM $\text{NaCl} + 25 \text{ mM } \text{Na}_2\text{SO}_4$ at pH 3.0 were prepared and treated in the flow plant by EO with an Ir-Sn-Sb oxide/stainless steel reactor at $j = 50 \text{ mA cm}^{-2}$ and liquid flow rate of 200 L h^{-1} for 360 min. The starting reddish solutions turned black during electrolysis, probably due to the formation of highly colored polymeric products, becoming almost colorless at long time only in the mixed electrolyte. In these trials, the pH was not regulated because it did not vary significantly, just diminishing to a value near 2.8 at the end of the treatments. This suggests the production of acidic by-products like final short-chain linear carboxylic acids in all media [4,21,23,30].

Fig. 2a presents the percentage of color removal at $\lambda = 437 \text{ nm}$ against electrolysis time for the above assays. The decolorization was strongly inhibited in the 50 mM NaClO_4 and 50 mM Na_2SO_4 solutions, only achieving 22.1% and 26.2% color removal, respectively. This means that the main oxidant in both cases, namely chemisorbed $\text{M}(\bullet\text{OH})$ generated at the Ir-Sn-Sb oxide anode surface, has a very low ability to remove the solution color at that wavelength, which can be related to either a low degradation rate of the dye with these radicals or the generation of large quantities of more recalcitrant colored by-products that interfere in the absorbance measurements, as suggested by the solution darkening. In contrast, the dye solution in 35 mM $\text{NaCl} + 25 \text{ mM } \text{Na}_2\text{SO}_4$ was continuously decolorized up to achieving 96.5% color reduction, in correspondence to an almost colorless final solution. This indicates that the active chlorine formed from Reactions (2) and (3) is able to quantitatively destroy the dye and its colored by-products, making the EO process efficient for decolorization.

The above absorbance decays were analyzed by kinetic equations related to simple reaction orders. No kinetic relationship was valid for describing the trends in NaClO_4 and Na_2SO_4 media, whereas an excellent pseudo-first-order equation relating $\ln(A_0/A)$ with t was followed in the mixed Cl^- -containing electrolyte, as can be seen in Fig. 2b. The slope of this plot is the apparent rate constant for decolorization (k_{dec}), with a value of 0.0071 min^{-1} and an R -squared of 0.991 at 200 L h^{-1} . This behavior suggests the attack of a constant concentration of the prevailing active chlorine species (HClO) over colored pollutants in the bulk.

An opposite tendency was obtained for the TOC decay of the 0.46 mM dye solution (100 mg L^{-1} TOC). After 360 min of electrolysis at $j = 50 \text{ mA cm}^{-2}$ and liquid flow rate of 60 L h^{-1} , about 20–21% TOC removal was found in NaClO_4 and Na_2SO_4 media, but only 7.5% TOC was reduced using the mixed electrolyte. This finding demonstrates the higher oxidation ability of $\text{M}(\bullet\text{OH})$ compared to active chlorine to mineralize the dye solution, which can be associated with a large production of refractory chloroderivatives in 35 mM $\text{NaCl} + 25 \text{ mM } \text{Na}_2\text{SO}_4$ to yield a largely persistent mixture of organic compounds. These by-products are colorless, unlike those produced under the attack of $\text{M}(\bullet\text{OH})$, which explains the almost total decolorization attained in the presence of Cl^- ion.

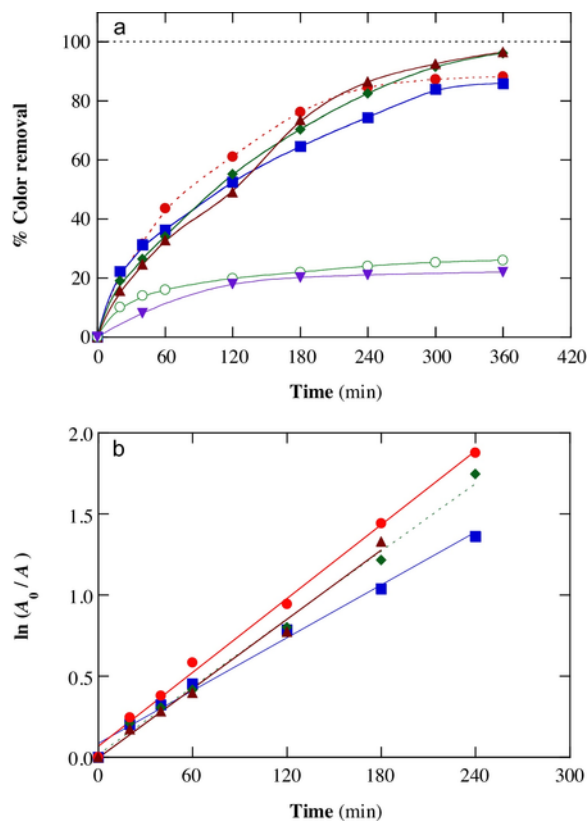


Fig. 2. (a) Change of percentage of color removal with electrolysis time for the electro-oxidation treatment of 2.5 L of a solution with 0.46 mM Acid Yellow 36 at pH 3.0 and $30 \text{ }^\circ\text{C}$ in the flow plant at $j = 50 \text{ mA cm}^{-2}$. Medium: (\blacktriangledown) 50 mM NaClO_4 and (\circ) 50 mM Na_2SO_4 at 200 L h^{-1} , or 35 mM $\text{NaCl} + 25 \text{ mM } \text{Na}_2\text{SO}_4$ at liquid flow rate: (\bullet) 60 L h^{-1} , (\blacksquare) 120 L h^{-1} , (\blacklozenge) 150 L h^{-1} and (\blacktriangle) 200 L h^{-1} . (b) Pseudo-first-order kinetics for the decolorization processes in 35 mM $\text{NaCl} + 25 \text{ mM } \text{Na}_2\text{SO}_4$. (For interpretation of the references to colour in this figure legend, the reader is referred to the web version of this article.)

From the above results, the quickest decolorization of the dye solution was achieved in 35 mM $\text{NaCl} + 25 \text{ mM } \text{Na}_2\text{SO}_4$. This medium was then selected to examine the influence of the main operation variables on the EO treatment in the flow plant.

3.4. Effect of operation variables on acid yellow 36 electro-oxidation in the mixed electrolyte

The liquid flow rate is an important variable in EO because it determines the mass transport of the reactants toward the anode as well as the oxidation rate of both, Cl^- and active chlorine. The effect of this parameter was examined for the degradation of 0.46 mM Acid Yellow 36 in the mixed electrolyte at pH 3.0 and $j = 50 \text{ mA cm}^{-2}$. As can be seen in Fig. 2a, a quite similar decolorization rate was obtained under all conditions tested, finally attaining 88.2%, 86.1%, 96.1% and 96.5% color abatement at increasing volumetric flow rates of 60, 120, 150 and 200 L h^{-1} (linear velocity of the liquid of 9.25, 18.52, 23.15 and 30.86 cm s^{-1}). The two higher liquid flow rates showed the largest decolorization, although the color disappearance always followed analogous trends. This is indicative of the pre-eminent reaction of the dye and its colored by-products with active chlorine in the bulk, with little influence of the mass transport of Cl^- ions toward the Ir-Sn-Sb oxide anode surface to be oxidized via Reaction (2). Fig. 2b shows the good straight lines determined for these trials assuming that the absorbance decay at $\lambda = 437 \text{ nm}$ obeyed a pseudo-

first-order kinetics. Table 2 summarizes the similar k_{dec} values thus calculated with $R^2 > 0.990$ in all cases. An average k_{dec} value of $0.0073 \pm 0.0002 \text{ min}^{-1}$ was obtained at $j = 50 \text{ mA cm}^{-2}$, disregarding the slightly lower value obtained at 120 L h^{-1} . In contrast, Table 2 shows a progressive enhancement in TOC reduction at higher liquid flow rate from 7.5% at 60 L h^{-1} to 18.0% at 200 L h^{-1} , resulting in raising MCE values from 4.0% to 9.5%. The improvement of mineralization as the liquid flow rate grew can be accounted for by: (i) the smaller contribution of parasitic Reactions (11)–(13) at the anode because of the shorter residence time of the liquid in the electrochemical reactor, in agreement with its higher linear velocity, and/or (ii) the enhanced mass transport of organic molecules toward the anode surface. Consequently, the reaction between organics and generated active chlorine in the large solution volume of the reservoir as well as that with $\bullet\text{OH}$ at the anode are promoted. According to these findings, a liquid flow rate of 200 L h^{-1} was chosen to investigate the effect of j and dye concentration on the performance of the EO process.

Fig. 3a highlights the gradual upgrading of color loss from a 0.46 mM dye solution in the mixed electrolyte when j rose from 20 to 150 mA cm^{-2} . After 360 min of electrolysis, 91.4% and 96.5% color decay were attained at 20 and 50 mA cm^{-2} , respectively, whereas total decolorization was achieved at that time at 100 mA cm^{-2} and in only 240 min operating at 150 mA cm^{-2} . This tendency can be ascribed to the progressively larger production of active chlorine as result of the acceleration of Cl^- oxidation at the anode from Reaction (2). The excellent linear $\ln(A_0/A)$ - t plots obtained for these trials are depicted in Fig. 3b. The k_{dec} values then increased from 0.0061 to 0.021 min^{-1} , with $R^2 > 0.987$, as can be seen in Table 2. The data given in this table also show a growing TOC abatement from 13.2% to 28.7% upon a j increase from 20 to 150 mA cm^{-2} , in agreement with the larger production of both, active chlorine and $\bullet\text{OH}$. In contrast, the opposite trend can be observed for the corresponding MCE values, which dropped from 17.4% to 5.0% within that j -range. This behavior can be related to a progressive loss of the relative amount of: (i) active chlorine accumulated, due to the larger extent of its parasitic Reactions (11)–(13), and (ii) $\bullet\text{OH}$ at the anode surface, as a result of self-destruction reactions. All this eventually diminishes the destruction of organics, making the EO process more inefficient. This

also agrees with the low rise (3.4-fold) of k_{dec} for a 7.5-fold growth of j (see Table 2).

The oxidation power of EO was further explored for dye contents between 0.23 and 0.92 mM in the mixed electrolyte at pH 3.0, $j = 150 \text{ mA cm}^{-2}$ and liquid flow rate of 200 L h^{-1} . In these assays, the decay of the dye concentration was determined by reversed-phase HPLC. Fig. 4 reveals the complete dye disappearance at increasing times of 40, 90 and 180 min for 0.23, 0.46 and 0.92 mM , respectively. This is the expected trend when an almost constant amount of oxidant is generated in the system, thus requiring a larger timer to remove greater amounts of the dye. The inset of Fig. 4 presents the good linear correlations found for the concentration decays assuming a pseudo-first-order oxidation reaction for Acid Yellow 36. The apparent rate constant for dye removal (k_1) decreased from 0.146 min^{-1} at 0.23 mM (87 mg L^{-1} TOC) to 0.022 min^{-1} at 0.92 mM (347 mg L^{-1} TOC), as can be seen in Table 2. This means that the dye decay did not actually agree with a pseudo-first-order process because in such a case, k_1 should be independent of the initial concentration. Nevertheless, this behavior corroborates the reaction of the dye molecules with a constant concentration of active chlorine species at each Acid Yellow 36 concentration, and suggests a complex process since oxidants not only react with the dye, but also with its oxidation by-products. Comparison of the results for the 0.46 M solution of Figs. 3a and 4 allows inferring that decolorization was much slower than the dye abatement, with $k_{\text{dec}} = 0.021 \text{ min}^{-1} < k_1 = 0.056 \text{ min}^{-1}$. This suggests the formation of large amounts of colored by-products that are more slowly destroyed by active chlorine than the dye. In addition, a closer look to Table 2 reveals a decrease of the percentage of TOC removal from 40.0% at 0.23 mM to 18.5% at 0.92 mM , as expected from the presence of greater organic load. However, the MCE values underwent a progressive enhancement from 3.5% to 6.6%, which may be explained by the smaller extent at which parasitic reactions occur because of the enhancement of positive reaction events between the organics and the oxidants, thereby causing larger TOC abatements.

From this subsection, one can establish that the most efficient EO treatment of Acid Yellow 36 is achieved operating at low j values and high dye contents, although in all cases a partial mineralization was found using an Ir-Sn-Sb oxide anode.

Table 2

Percentage of color or dye removal, along with the corresponding apparent rate constants and their R -squared, percentage of TOC decay and mineralization current efficiency after 360 min of electro-oxidation of 2.5 L of Acid Yellow 36 solutions in $35 \text{ mM NaCl} + 25 \text{ mM Na}_2\text{SO}_4$ at pH 3.0 in a flow plant using an Ir-Sn-Sb oxide anode under different experimental conditions.

[dye] (mg L^{-1})	$[\text{Fe}^{2+}]$ (mM)	j (mA cm^{-2})	Liquid flow rate (L h^{-1})	k (min^{-1})	R^2	% color removal	% TOC removal	MCE (%)
87	–	150	200	0.146 ^a	0.988	– ^c	40.0	3.5
173	–	20	200	0.0061 ^b	0.993	91.4	13.2	17.4
173	–	50	60	0.0075 ^b	0.996	88.2	7.5	4.0
173	–	50	120	0.0054 ^b	0.990	85.9	9.2	4.8
173	–	50	150	0.0070 ^b	0.995	96.1	17.9	9.4
173	–	50	200	0.0071 ^b	0.991	96.5	18.0	9.5
173	–	100	200	0.013 ^b	0.994	100	21.0	5.5
173	–	150	200	0.056 ^a 0.021 ^b	0.987	100 ^d	28.7	5.0
					0.998			
173	1 mM	150	200	0.068 ^a	0.996	100 ^e	33.0	5.8
				0.038 ^b	0.989			
173	1 mM + UVA	150	200	0.067 ^a	0.994	100 ^e	36.8	6.5
				0.043 ^b	0.990			
357	–	150	200	0.022 ^a	0.997	– ^c	18.5	6.6

^a Pseudo-first-order rate constant for dye removal (k_1).

^b Pseudo-first-order rate constant for decolorization (k_{dec}).

^c Not determined.

^d At 240 min.

^e At 120 min.

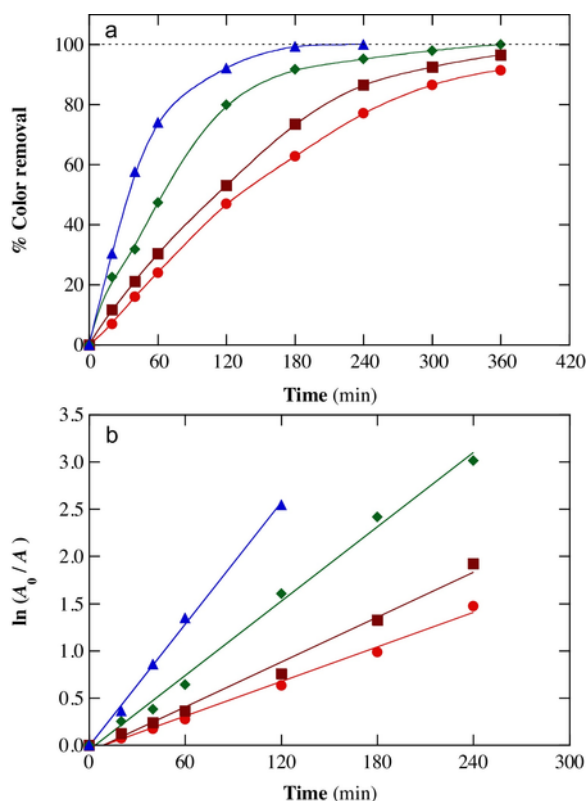


Fig. 3. (a) Effect of current density on the percentage of color removal with electro-oxidation time for the electro-oxidation treatment of 2.5 L of 0.46 mM Acid Yellow 36 solution in 35 mM NaCl + 25 mM Na₂SO₄ at pH 3.0 and 30 °C in the flow plant at 200 L h⁻¹. Current density: (●) 20 mA cm⁻², (■) 50 mA cm⁻², (◆) 100 mA cm⁻² and (▲) 150 mA cm⁻². (b) Kinetic analysis considering a pseudo-first-order decolorization reaction. (For interpretation of the references to colour in this figure legend, the reader is referred to the web version of this article.)

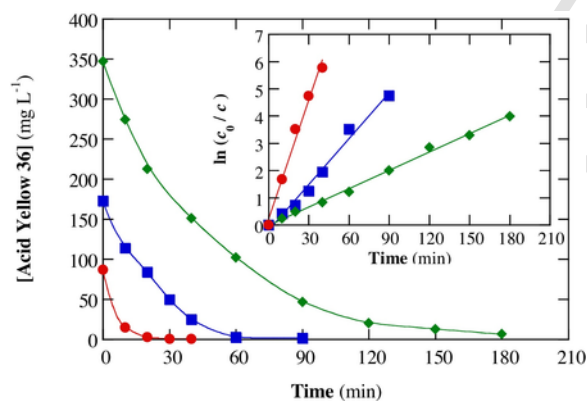


Fig. 4. Concentration dye decay vs. electrolysis time treating 2.5 L of (●) 0.23 mM, (■) 0.46 mM and (◆) 0.92 mM Acid Yellow 36 solutions in 35 mM NaCl + 25 mM Na₂SO₄ at pH 3.0 and 30 °C by electro-oxidation in the flow plant at $j = 150 \text{ mA cm}^{-2}$ and liquid flow rate of 200 L h⁻¹. The inset panel presents the corresponding kinetic analysis considering a pseudo-first-order reaction for the dye. (For interpretation of the references to colour in this figure legend, the reader is referred to the web version of this article.)

3.5. Fenton-like process in the mixed electrolyte

The results obtained in previous subsections lay the foundations to clarify if a Fenton-like process involving $\bullet\text{OH}$ generation from Reaction (5) can occur in the presence of Fe^{2+} in the mixed electrolyte. To this aim, 2.5 L of a 0.46 mM dye solution in 35 mM NaCl + 25 mM Na₂SO₄ with 1.0 mM Fe^{2+} at pH 3.0 were electrolyzed in the flow plant operating at $j = 150 \text{ mA cm}^{-2}$ and liquid flow rate 200 L h⁻¹. These assays were performed without and with UVA irradiation, i.e., under EF-like and PEF-like conditions, respectively. A slight acidification to pH 2.7–2.8 was observed after 360 min of both treatments.

Fig. 5a demonstrates a clear enhancement of the percentage of color removal in the EF-like and PEF-like treatments as compared to the EO (i.e., in the absence of Fe^{2+}). In the latter case, a time of 240 min was required to attain total decolorization at $\lambda = 437 \text{ nm}$, whereas in both EF-like and PEF-like processes, the color disappeared at a shorter time of ca. 120 min. The quicker decolorization in the two latter cases can then be ascribed to the faster destruction of the dye and its colored by-products in the bulk under the competitive action of active chlorine formed from Reactions (2) and (3) and homogeneous $\bullet\text{OH}$ originated from the Fenton-like Reaction (5). It is noteworthy that Fig. 5a reveals just a slight acceleration of the color removal in the PEF-like process if compared to the EF-like one, suggesting a minor contribution of additional $\bullet\text{OH}$ induced by the photolytic Reaction (7) to dye degradation, along with photostability of the dye and its colored by-products. A pseudo-first-order equation was verified for all absorbance decays at $\lambda = 437 \text{ nm}$, as can be seen in Fig. 5b and Table 2. As expected, the k_{dec} value for the PEF-like treatment (0.043 min^{-1}) was only slightly higher than that of the EF-like one (0.038 min^{-1}), being both values much greater than that of the EO process (0.021 min^{-1}).

A similar comparative profile was found for the removal of the dye concentration. Fig. 5c highlights a quite similar dye decay in both Fenton-like processes, being much more rapid than that in EO. Total dye disappearance was attained after 60 and 90 min of electrolysis, which were much shorter times than those needed for total decolorization (see Fig. 5a). This finding corroborates the generation of colored by-products that hamper the loss of solution color. From the pseudo-first-order relationships followed by the above concentration decays and presented in the inset of Fig. 5c, a $k_1 = 0.067 \pm 0.001 \text{ min}^{-1}$ was determined for both, EF-like and PEF-like treatments, a value higher than 0.056 min^{-1} obtained for EO (see Table 2). The fact that the dye was removed with same k_1 -value for both Fenton-like processes confirms that the production of $\bullet\text{OH}$ by the photolytic Reaction (7) was really small. This allows concluding that UVA light can basically serve to induce the photodegradation of some colored by-products to yield a slightly faster decolorization in the PEF-like process.

The aforementioned results suggest the existence of the Fenton-like Reaction (5) that allows the generation of $\bullet\text{OH}$ and hence, it accelerates the dye and color removal. Additional confirmation of this reaction was found from the corresponding percentage of TOC removal after 360 min of electrolysis, listed in Table 2. This value grew from 28.7% in EO to 33.0% in EF-like and 36.8% in PEF-like processes, with the concomitant rise in MCE. The greater decontamination by the EF-like treatment compared to the EO one can be associated with the extra $\bullet\text{OH}$ production via the Fenton-like Reaction (5), which accelerates the mineralization of by-products generated. However, the high stability of intermediates, especially those complexed with Fe(III), impedes a more pronounced enhancement. In contrast, the superior oxidation ability of the PEF-like process can be

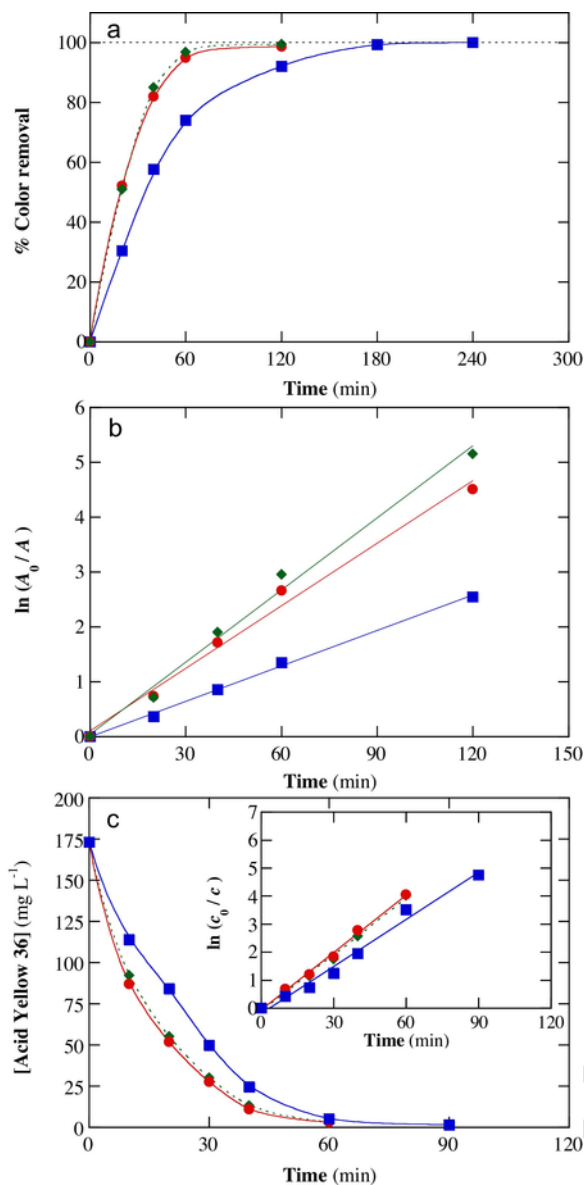


Fig. 5. (a) Variation of the percentage of color removal with electrolysis time for the electro-oxidation of 2.5 L of 0.46 mM Acid Yellow 36 solutions in 35 mM NaCl + 25 mM Na₂SO₄ (■) without Fe²⁺ addition and with (●) 1.0 mM Fe²⁺ (EF-like process) or (◆) 1.0 mM Fe²⁺ + UVA irradiation (PEF-like process) at pH 3.0 and 30 °C in the flow plant at $j = 150 \text{ mA cm}^{-2}$ and liquid flow rate of 200 L h⁻¹. (b) Pseudo-first-order kinetic analysis for the three decolorization processes. (c) Dye concentration decay for the same assays. The kinetic analysis assuming a pseudo-first-order reaction for Acid Yellow 36 is shown in the inset panel. (For interpretation of the references to colour in this figure legend, the reader is referred to the web version of this article.)

related to the production of more $\bullet\text{OH}$ from Reaction (5) and the additional photolysis of certain refractory by-products, including Fe(III) complexes, upon the action of UVA radiation, thus enhancing the mineralization process [15,24,30].

3.6. Detection of final carboxylic acids and fate of inorganic ions

Ion-exclusion HPLC analysis of the 0.46 mM dye solution in mixed electrolyte treated by EO and EF-like processes revealed the formation of maleic and acetic acids. It is known that both carboxylic acids are generated from the oxidative cleavage of the aromatic rings

of Acid Yellow 36 [4,15], being the acids transformed into the final oxalic and formic acids, which were not detected in the above trials. This fact suggests a preferential reaction of maleic and acetic acids with active chlorine, leading to chloroderivatives different from oxalic and formic acids. Fig. 6a shows a slow and continuous accumulation of maleic acid up to 3.5 and 2.4 mg L⁻¹ at the end of EO and EF-like treatments, whereas a larger content of 34.7 and 30.3 mg L⁻¹ was finally determined for acetic acid. Note that the accumulation of acetic acid began at much shorter times in the EF-like process due to the faster oxidation of some primary intermediates with additional $\bullet\text{OH}$ originated for Fenton-like Reaction (5). A simple mass balance revealed that the final solutions in such treatments contained 15.3 and 13.1 mg L⁻¹ of TOC, only representing 21.4% and 19.5% of the remaining organic load. Hence, a large quantity of other undetected persistent by-products was produced during the dye degradation in the mixed electrolyte.

To elucidate the nature of generated by-products, the inorganic ions lost or released after 360 min of EF-like degradation were determined. Fig. 6b shows a large removal of Cl⁻ from the starting mixed electrolyte since it was oxidized to HClO via Reactions (2) and (3), followed by oxidation of HClO to ClO₃⁻ and ClO₄⁻ from Reactions (11)–(13). No ClO₂⁻ was detected due to its instability in acidic conditions. Since the sum of ClO₃⁻ and ClO₄⁻ contents was 8.95 mM, a value lower than 9.86 mM Cl⁻ lost, one can infer that about 0.91 mM of chlorine was present in the final solution either as active chlorine or chloro-organics. Note that this value is lower than 1.27 mM of ac-

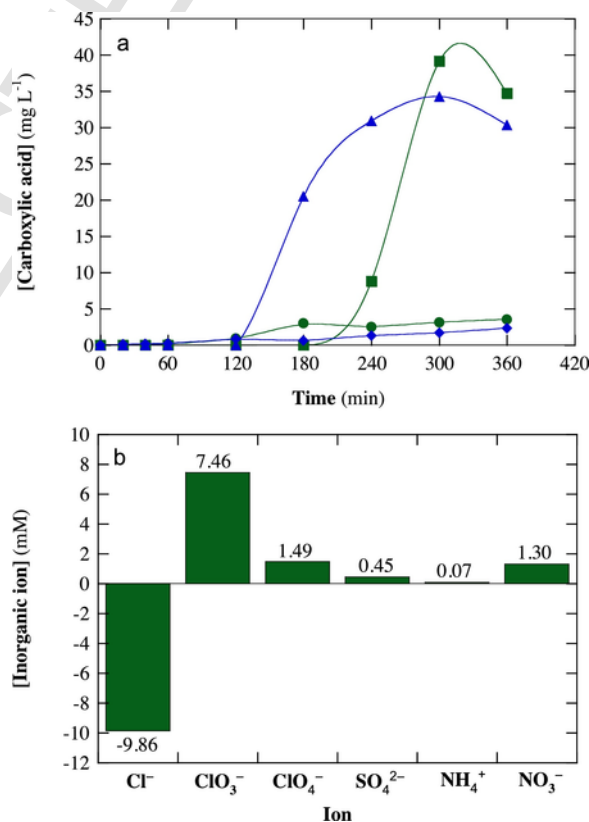


Fig. 6. (a) Time course of (●◆) maleic and (■▲) acetic acids detected during the electro-oxidation treatment of 2.5 L of 0.46 mM Acid Yellow 36 solutions in 35 mM NaCl + 25 mM Na₂SO₄ (●■) without Fe²⁺ addition or with (◆▲) 1.0 mM Fe²⁺ (EF-like process) at pH 3.0 and 30 °C using the flow plant at $j = 150 \text{ mA cm}^{-2}$ and liquid flow rate of 200 L h⁻¹. (b) Concentration of released or accumulated inorganic ions at 360 min for the EF-like trial. (For interpretation of the references to colour in this figure legend, the reader is referred to the web version of this article.)

tive chlorine found upon electrolysis of the raw background electrolyte under the same conditions (see Fig. 1b), thus confirming its ability to attack the dye and its by-products. It is also remarkable the overall conversion of the initial S of the dye (0.46 mM) into SO_4^{2-} and of its initial N (1.38 mM) pre-eminently as NO_3^- and, to a much slower extent, as NH_4^+ , as stated in Reaction (10). These findings confirm the loss of all the heteroatoms of the dye during its degradation and, consequently, linear chlorinated compounds and non-chlorinated carboxylic acids could be preferentially produced from the breaking of the benzenic moieties.

4. Conclusions

The Ir-Sn-Sb oxide anode prepared by the Pechini method showed a low production of chemisorbed $\text{M}(\bullet\text{OH})$, but a large ability to generate active chlorine (as HClO) in a Cl^- -containing electrolyte. A quick decolorization of Acid Yellow 36 solutions was found in this medium by EO due to action of HClO over the colored by-products, although the accumulation of chloroderivatives impeded the complete mineralization. In contrast, the color was poorly removed in NaClO_4 or Na_2SO_4 media because of the small contribution of $\text{M}(\bullet\text{OH})$. The liquid flow rate in the plant did not affect significantly the decolorization rate, but its increase caused a higher TOC removal due to the deceleration of parasitic reactions of active chlorine. This can also explain the better performance of the EO process with decreasing j and increasing dye concentration. The absorbance and dye concentration abatements obeyed a pseudo-first-order kinetics, with greater apparent rate constant in the latter case. The decolorization, dye concentration decay and TOC removal were enhanced by adding 1.0 mM Fe^{2+} to the dye solution in the mixed electrolyte, which is a clear evidence of the formation of $\bullet\text{OH}$ in the bulk from the Fenton-like reaction between generated HClO and added Fe^{2+} . The PEF-like treatment showed larger mineralization ability than the EF-like one by the additional photolysis of intermediates under UVA irradiation. Maleic and acetic acids were detected as final short-chain linear carboxylic acids. High contents of ClO_3^- and ClO_4^- were formed from HClO oxidation, whereas the initial S and N were transformed into SO_4^{2-} and NO_3^- , respectively.

Acknowledgements

Financial support from project CTQ2016-78616-R (MINECO, Feder, EU) is acknowledged. The authors would also like to thank financial support under project 240522 (CONACYT, Mexico) and project 869/2016 (University of Guanajuato, Mexico). Z. Aguilar is grateful to CONACYT for the PhD scholarship No. 421053 granted.

Appendix A. Supplementary data

Supplementary data associated with this article can be found, in the online version, at <http://dx.doi.org/10.1016/j.apcatb.2017.01.006>.

References

- [1] D. Rajkumar, J.G. Kim, *J. Hazard. Mater. B* 136 (2006) 203–212.
- [2] T. Robinson, G. McMullan, R. Marchant, P. Nigam, *Bioresour. Technol.* 77 (2001) 247–255.
- [3] E. Forgacs, T. Cserhati, G. Oros, *Environ. Int.* 30 (2004) 953–971.
- [4] E. Brillas, C.A. Martinez-Huitle, *Appl. Catal. B: Environ.* 166–167 (2015) 603–643.
- [5] H. Zollinger, *Color Chemistry: Synthesis, Properties, and Applications of Organic Dyes and Pigments*, VHCA and Wiley-VCH, Switzerland, 2003.
- [6] A.B. dos Santos, F.J. Cervantes, J.B. van Lier, *Bioresour. Technol.* 98 (2007) 2369–2385.
- [7] S.M.A.G. Ulson de Souza, E. Forgiarini, A.A. Ulson de Souza, *J. Hazard. Mater.* 147 (2007) 1073–1078.
- [8] K.P. Sharma, S. Sharma, S.P. Sharma, K. Singh, S. Kumar, R. Grover, P.K. Sharma, *Chemosphere* 69 (2007) 48–54.
- [9] V.J.P. Vilar, L.X. Pinho, A.M.A. Pintor, R.A.R. Boaventura, *Sol. Energy* 85 (2011) 1927–1934.
- [10] V. Khandegar, A.K. Saroha, *J. Environ. Manage.* 128 (2013) 949–963.
- [11] C. Saez, M. Panizza, M.A. Rodrigo, G. Cerisola, *J. Chem. Technol. Biotechnol.* 82 (2007) 575–581.
- [12] M. Villanueva-Rodriguez, A. Hernandez-Ramerez, J.M. Peralta-Hernandez, E.R. Bandala, M.A. Quiroz-Alfaro, *J. Hazard. Mater.* 167 (2009) 1226–1230.
- [13] A. Ozcan, M.A. Oturan, N. Oturan, Y. Sahin, *J. Hazard. Mater.* 163 (2009) 1213–1220.
- [14] K. Cruz-Gonzalez, O. Torres-Lopez, A. Garcıa-Leon, J.L. Guzman-Mar, L.H. Reyes, A. Hernandez-Ramerez, J.M. Peralta-Hernandez, *Chem. Eng. J.* 160 (2010) 199–206.
- [15] E.J. Ruiz, C. Arias, E. Brillas, A. Hernandez-Ramerez, J.M. Peralta-Hernandez, *Chemosphere* 82 (2011) 495–501.
- [16] S. Garcıa-Segura, F. Centellas, C. Arias, J.A. Garrido, R.M. Rodriguez, P.L. Cabot, E. Brillas, *Electrochim. Acta* 58 (2011) 303–311.
- [17] A.J. Mendez-Martinez, M.M. Davila-Jimenez, O. Ornelas-Davila, M.P. Elizalde-Gonzalez, U. Arroyo-Abad, I. Sires, E. Brillas, *Electrochim. Acta* 59 (2012) 140–149.
- [18] J.M. Aquino, R.C. Rocha-Filho, M.A. Rodrigo, C. Saez, P. Canizares, *Water. Air Soil Pollut.* 224 (2013) 1397–1406.
- [19] R. Chaiyont, C. Badoe, C. Ponce de Leon, J.L. Nava, F.J. Recio, I. Sires, P. Her-rasti, F.C. Walsh, *Chem. Eng. Technol.* 36 (2013) 123–129.
- [20] A. El-Ghenymy, F. Centellas, J.A. Garrido, R.M. Rodriguez, I. Sires, P.L. Cabot, E. Brillas, *Electrochim. Acta* 130 (2014) 568–576.
- [21] I. Sires, E. Brillas, M.A. Oturan, M.A. Rodrigo, M. Panizza, *Environ. Sci. Pollut. Res.* 21 (2014) 8336–8367.
- [22] A. Thiam, E. Brillas, F. Centellas, P.L. Cabot, I. Sires, *Electrochim. Acta* 173 (2015) 523–533.
- [23] C.A. Martinez-Huitle, M.A. Rodrigo, I. Sires, O. Scialdone, *Chem. Rev.* 115 (2015) 13362–13407.
- [24] A. Thiam, I. Sires, J.A. Garrido, R.M. Rodriguez, E. Brillas, *J. Hazard. Mater.* 290 (2015) 34–42.
- [25] T.X.H. Le, M. Bechelany, S. Lacour, N. Oturan, M.A. Oturan, M. Cretin, *Carbon* 94 (2015) 1003–1011.
- [26] A. Thiam, I. Sires, J.A. Garrido, R.M. Rodriguez, E. Brillas, *Sep. Purif. Technol.* 140 (2015) 43–52.
- [27] S. Shukla, M.A. Oturan, *Environ. Chem. Lett.* 13 (2015) 157–172.
- [28] A. Bedolla-Guzman, I. Sires, A. Thiam, J.M. Peralta-Hernandez, S. Gutierrez-Granados, E. Brillas, *Electrochim. Acta* 206 (2016) 307–316.
- [29] V.M. Vasconcelos, C. Ponce-de-Leon, J.L. Nava, M.R.V. Lanza, *J. Electroanal. Chem.* 765 (2016) 179–187.
- [30] F.C. Moreira, R.A.R. Boaventura, E. Brillas, V.J.P. Vilar, *Appl. Catal. B: Environ.* 202 (2017) 217–261.
- [31] B. Marselli, J. Garcıa-Gomez, P.A. Michaud, M.A. Rodrigo, C. Comninellis, *J. Electrochem. Soc.* 150 (2003) D79–D83.
- [32] M. Panizza, G. Cerisola, *Chem. Rev.* 109 (2009) 6541–6569.
- [33] G. Coria, I. Sires, E. Brillas, J.L. Nava, *Chem. Eng. J.* 304 (2016) 817–825.
- [34] E. Butron, M.E. Juarez, M. Solis, M. Teutli, I. Gonzalez, J.L. Nava, *Electrochim. Acta* 52 (2007) 6888–6894.
- [35] J.L. Nava, F. Nunez, I. Gonzalez, *Electrochim. Acta* 52 (2007) 3229–3235.
- [36] W. Wu, Z.H. Huang, T.T. Lim, *Appl. Catal. A: Gen.* 480 (2014) 58–78.
- [37] D.Z. Mijjin, M.L. Avramov-Ivic, A.E. Onjia, B.N. Grgur, *Chem. Eng. J.* 204–206 (2012) 151–157.
- [38] M.I. Leon, Z.G. Aguilar, J.L. Nava, *J. Electrochem. Sci. Eng.* 4 (2014) 247–258.
- [39] N. Kishimoto, Y. Nakamura, M. Kato, H. Otsu, *Chem. Eng. J.* 260 (2015) 590–595.
- [40] L.P. Candeias, M.R.L. Stanford, P. Wardman, *Free Radic. Res.* 20 (1994) 241–249.
- [41] A. Thiam, I. Sires, E. Brillas, *Water Res.* 81 (2015) 178–187.
- [42] S. Chen, Y. Zheng, S. Wang, X. Chen, *Chem. Eng. J.* 172 (2011) 47–51.
- [43] P.K. Malik, *Dyes Pigments* 56 (2003) 239–249.
- [44] A. Mittal, V.K. Gupta, A. Malviya, J. Mittal, *J. Hazard. Mater.* 151 (2008) 821–832.
- [45] S. Mozia, A.W. Morawski, M. Toyoda, T. Tsumura, *Chem. Eng. J.* 150 (2009) 152–159.
- [46] A.R. Khataee, M. Safarpour, M. Zarei, S. Aber, *J. Mol. Catal. A: Chem.* 363–364 (2012) 58–68.
- [47] S. Khezrianjoo, H.D. Revanasiddappa, *J. Catal.* (2013) 582058 (7 pp).
- [48] H. Aghdasinia, R. Bagheri, B. Vahid, A. Khataee, *Environ. Technol.* 37 (2016) 2703–2712.

- [49] J. Macías-Sánchez, L. Hinojosa-Reyes, J.L. Guzmán-Mar, J.M. Peralta-Hernández, A. Hernández-Ramírez, *Photochem. Photobiol. Sci.* 10 (2011) 332–337.
- [50] Y. Juang, E. Nurhayati, C. Huang, J.R. Pan, S. Huan, *Sep. Purif. Technol.* 120 (2013) 289–295.
- [51] K. Cruz-González, O. Torres-López, A.M. García-León, E. Brillas, A. Hernández-Ramírez, J.M. Peralta-Hernández, *Desalination* 286 (2012) 63–68.
- [52] M.P. Pechini, US Patent 3330697 A (1967).
- [53] B. Borbón, M.T. Oropeza-Guzman, E. Brillas, I. Sirés, *Environ. Sci. Pollut. Res.* 21 (2014) 8573–8584.
- [54] APWA, AWWA, WEF, *Standard Methods for the Examination of Water and Wastewater*, 21 st Ed. Method Number 4500-Cl Chlorine (residual)—G. DPD Colorimetric Method, American Public Health Association, Washington D.C, 2005. pp. 4–67–4-68..
- [55] X. Chen, G. Chen, P.L. Yue, *J. Phys. Chem. B* 105 (2001) 4623–4628.
- [56] S. Chen, Y. Zheng, S. Wang, X. Chen, *Chem. Eng. J.* 172 (2011) 47–51.

UNCORRECTED PROOF